

# Optical Engineering

[SPIDigitalLibrary.org/oe](http://SPIDigitalLibrary.org/oe)

## **Simulation and modeling of laser range profiling and imaging of small surface vessels**

Ove Steinvall  
Tomas Chevalier  
Christina Grönwall

# Simulation and modeling of laser range profiling and imaging of small surface vessels

Ove Steinvall,<sup>a,\*</sup> Tomas Chevalier,<sup>b</sup> and Christina Grönwall<sup>c</sup>

<sup>a</sup>Electro-Optical Systems, Swedish Defense Research Agency (FOI), Box 1165, 581 11 Linköping, Sweden

<sup>b</sup>Informatics Group, Swedish Defense Research Agency (FOI), Box 1165, 581 11 Linköping, Sweden

<sup>c</sup>Saab Aeronautics, Swedish Defense Research Agency (FOI), Box 1165, 581 11 Linköping, Sweden

**Abstract.** The detection and classification of small surface targets at long ranges is a growing need for naval security. Simulations of a laser radar at 1.5  $\mu\text{m}$  aimed for search, detect, and recognition of small maritime targets will be discussed. The data for the laser radar system will be based on present and realistic future technology. The simulated data generate signal waveforms for every pixel in the sensor field-of-view. From these we can also generate two-dimensional (2-D) and three-dimensional (3-D) range and intensity images. The simulations will incorporate typical target movements at different sea states, vessel courses, effects of the atmospheric turbulence and also include different beam jitter. The laser pulse energy, repetition rate as well as the receiver and detector parameters have been the same during the simulations. We have also used a high resolution (sub centimeter) laser radar based on time correlated single photon counting to acquire examples of range profiles from different small model ships. The collected waveforms are compared with simulated wave forms based on 3-D models of the ships. A discussion of the classification potential based on information in 1-D, 2-D, and 3-D data separately and in combination is made versus different environmental conditions and system parameters. © The Authors. Published by SPIE under a Creative Commons Attribution 3.0 Unported License. Distribution or reproduction of this work in whole or in part requires full attribution of the original publication, including its DOI. [DOI: [10.1117/1.OE.53.1.013109](https://doi.org/10.1117/1.OE.53.1.013109)]

Keywords: range-gated imaging; burst illumination; three-dimensional; ladar; small boats; laser signatures.

Paper 131555P received Oct. 9, 2013; revised manuscript received Dec. 22, 2013; accepted for publication Dec. 30, 2013; published online Feb. 3, 2014; corrected Feb. 7, 2014.

## 1 Introduction

The interest in novel solutions for improved Maritime Domain Awareness has seen an increase in recent years.<sup>1</sup> Persistent detection, positioning, tracking, and possibly identification, of small surface targets, like small boats at sea and in littoral waters, have become important capabilities for countering illegal immigration, piracy, drug trafficking, and asymmetric threats. Applications exist also in a number of neighboring areas, such as search and rescue at sea and detection of ice hazards.

Traditional systems (navigation radar and passive optical systems) do not yield satisfactory performance for small vessels under all weather and lighting conditions due to limitations in sensitivity, clutter performance, and resolution. Furthermore, wide area sensors such as radar have limited capability to classify and identify targets, while many optical sensors capable of identification and classification suffer from severely limited capability to cover larger areas in a limited time interval.

In order to attempt to overcome some limitations of currently available systems, Swedish Defense Research Agency (FOI) has undertaken work to design and test a prototype sensor system consisting of a radar sensor working in cooperation with a laser system capable of making both range profiling and range gated imaging.<sup>2</sup> We can also incorporate passive electro-optical (EO) systems in the visual and infrared wavelength regions for an increased support of the detection, tracking and identification (ID) capability.

Identification of ships is usually done by passive imaging. Krapels et al.<sup>3</sup> describe the difficulty to identify small maritime vessels in the visible and mid IR bands. de Jong et al.<sup>4</sup> investigated optical characteristics of small surface targets, using a hyperspectral camera, a polarization-sensitive camera and a camera with high resolution all working in the visible band. The targets showed a positive and a negative contrast element in contrary to the imagery from thermal IR sensors, for which the contrast is almost always positive. In a similar paper, Schwering et al.<sup>5</sup> used a number of cameras working both in the visible, near infrared (NIR), midwave infrared (MWIR), and long-wave infrared (LWIR) bands. At longer ranges and in coastal environments these target signals may well be hidden within the background clutter.

Active imaging of maritime targets have been reported by Bonnier et al.<sup>6</sup> and David et al.<sup>7</sup> using NIR wavelengths and by our group at FOI<sup>8</sup> using as well as IOSB in Germany<sup>9</sup> both using 1.5- $\mu\text{m}$  range gated systems. Recently, an analysis of full three-dimensional (3-D) imaging (flash imaging) data using a focal plane array enabling 3-D imaging in one laser pulse has been reported by Armbruster and Hammer.<sup>10</sup> The basic advantage of using full range imagery is that object recognition can be reliably automated, even for noncontrolled environments such as outdoor scenes with variable background illumination.

However, long range ID or ID at closer range of very small targets has its limitations for imaging due to the demand on transverse sensor resolution. It is therefore a motivation to look for one-dimensional (1-D) laser techniques also for target ID. These include vibrometry<sup>11</sup> and laser range profiling including its extension to tomography. Vibrometry can give good results, but is also sensitive to

\*Address all correspondence to: Ove Steinvall, E-mail: [oveste@foi.se](mailto:oveste@foi.se)

certain vibrating parts on the target being in the field-of-view (FOV).

Laser range profiling is attractive because the maximum range can be substantial, especially for a small beam width. A range profiler can also be used in a scanning mode to detect targets within a certain sector. The same laser can also be used for active imaging when the target comes closer and is angularly resolved. Laser range profiling has been tested for both search and ID of small surface targets<sup>12,13</sup> and also for aircraft ID.<sup>14</sup> A recent article by Schoemaker and Benoist<sup>15</sup> discusses laser range profiling of small maritime targets in relation to a NATO trial in San Diego.

This paper will show simulation results for laser range profiling and imaging of small boat models under different environmental conditions and discuss the results from a system perspective. Recently, we showed by simulations and laboratory measurements that laser range profiling is a promising method of identification of small sea surface targets at long ranges.<sup>16</sup> The influence on the range profiles from target tip due to waves from different aspect angles was investigated. It was shown that the range profile is rather stable if one compensates for the aspect angle. The profiling capability may be combined with active imaging. Using an eye safe wavelength of  $1.5 \mu\text{m}$  is especially favorable

due to the low water backscatter at this wavelength. This has been verified by our group in other experiments.<sup>8</sup>

We will start by a short description of the modeling efforts including digital boat models. Then we will describe simulation of two models, a fishing boat and a small row-boat, concerning range profiling and also show laboratory measurements of the real models of the boats. Then we will extend the simulation to more boat types and different environmental conditions, such as sea state, atmospheric turbulence, and range [leading to different signal-to-noise ratios (SNR)]. Analysis is concentrated on range profiles but the 2-D intensity, and 3-D data are also exemplified as are the preliminary investigation of data processing for automatic target classification.

## 2 Modeling Efforts

The FOI has developed a model called FOI-LadarSim to simulate complex 3-D ladar systems.<sup>17</sup> It is a model that combines imaging of advanced scenario setups with atmospheric turbulence modeling as well as allowing degrading sensor effects to affect the resulting data. The FOI-LadarSim is part of a larger effort in ladar modeling of both soft and hard targets at FOI.<sup>18,19</sup> We have used the FOI-LadarSim model for investigating the laser range profiled for ships.

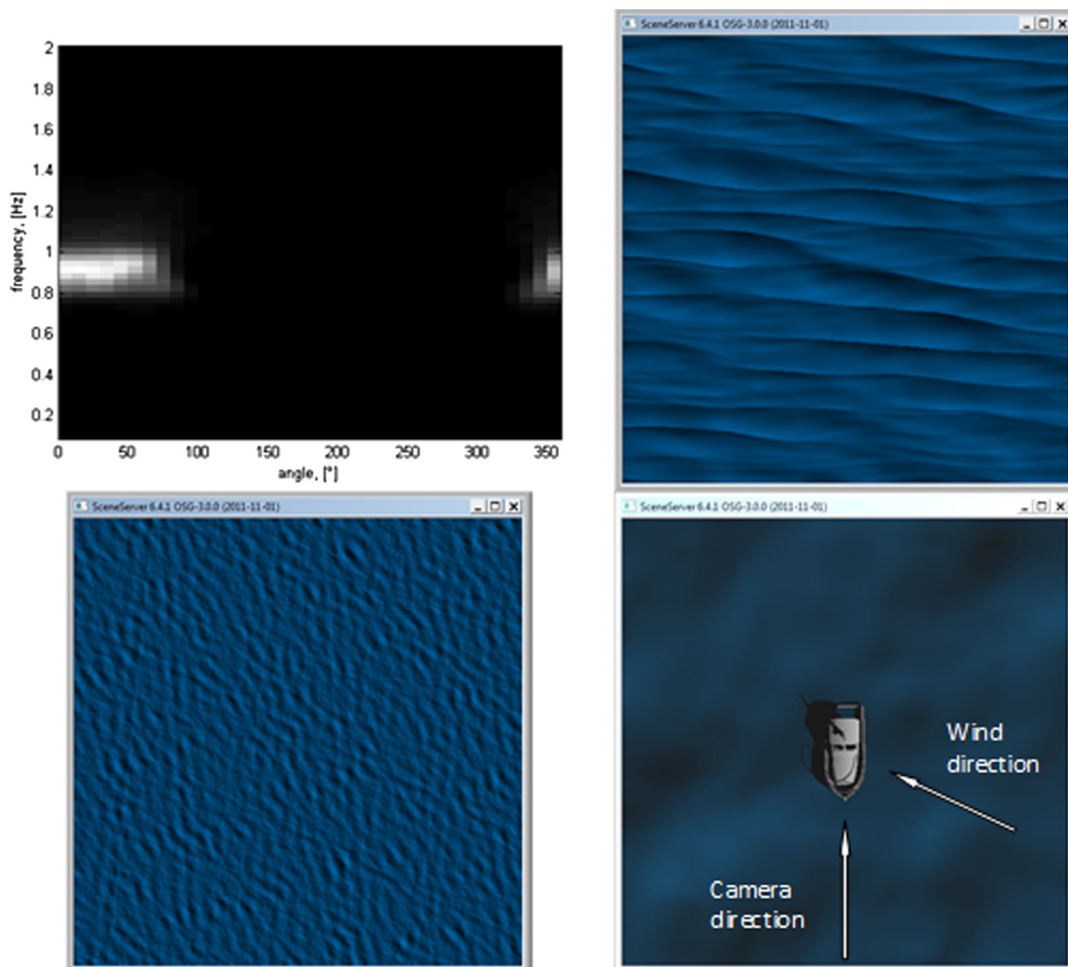


**Fig. 1** One of the wave situations simulated in the paper, where the wind speed is set to 10 m/s. (a) The spectrum, where the angle axis is defined as 0 deg when wind blows from east/right. White values correspond to high wave amplitudes. (b) Enlargement of the waves, while (c) is the same waves seen from the top. (d) The definition of the wind direction compared to the camera direction.



**Fig. 2** Toy model of a 43-cm long and 13-cm wide fishing boat. (a) A photo, and (b) a simplified three-dimensional (3-D) model (without sails and connecting ropes) used for simulating the waveform return from a laser profiling system. The model did not take into account any differences in reflectivity from the various parts of the boat.

By altering the sensor characteristics, the atmosphere, the target structure and its reflectivity distribution, and the aspect angles including water wave influence, we will be able to estimate the potential of laser range profiling ID for a great number of targets types' sensor characteristics and environmental conditions. This type of modeling can then guide the hardware development.

Focus for the model upgrades in this work was put on the wave simulations and on the boat modeling. The wave simulations were implemented using SWAN (SWAN Cycle III version 40.91A), which is a third-generation wave model, developed at Delft University of Technology,<sup>20</sup> that computes random, short-crested wind-generated waves. Based on environment settings such as wind speed and direction, SWAN generates a frequency spectrum for a number of directions. Using this spectrum, time resolved waves were generated by summing up the waves for each frequency and each direction. Figure 1 shows an example of spectrum and corresponding wave situation for a wind speed of 10 m/s. Three situations were prepared to be used in the boat simulations. All settings but the windspeed were constant for these three cases, and we assumed 10-m deep water, stationary waves, frequency vector defined with 36 steps between 0.1 and 2 Hz, and directional resolution of 10 deg. The direction of the wind was set to 300 deg, using the definition of 0 deg for the camera direction, as can be seen in Fig. 1. The only varied parameter was the wind speed, which was set to 2, 5, and 10 m/s, respectively. The results of the wave simulations were obtained for waves

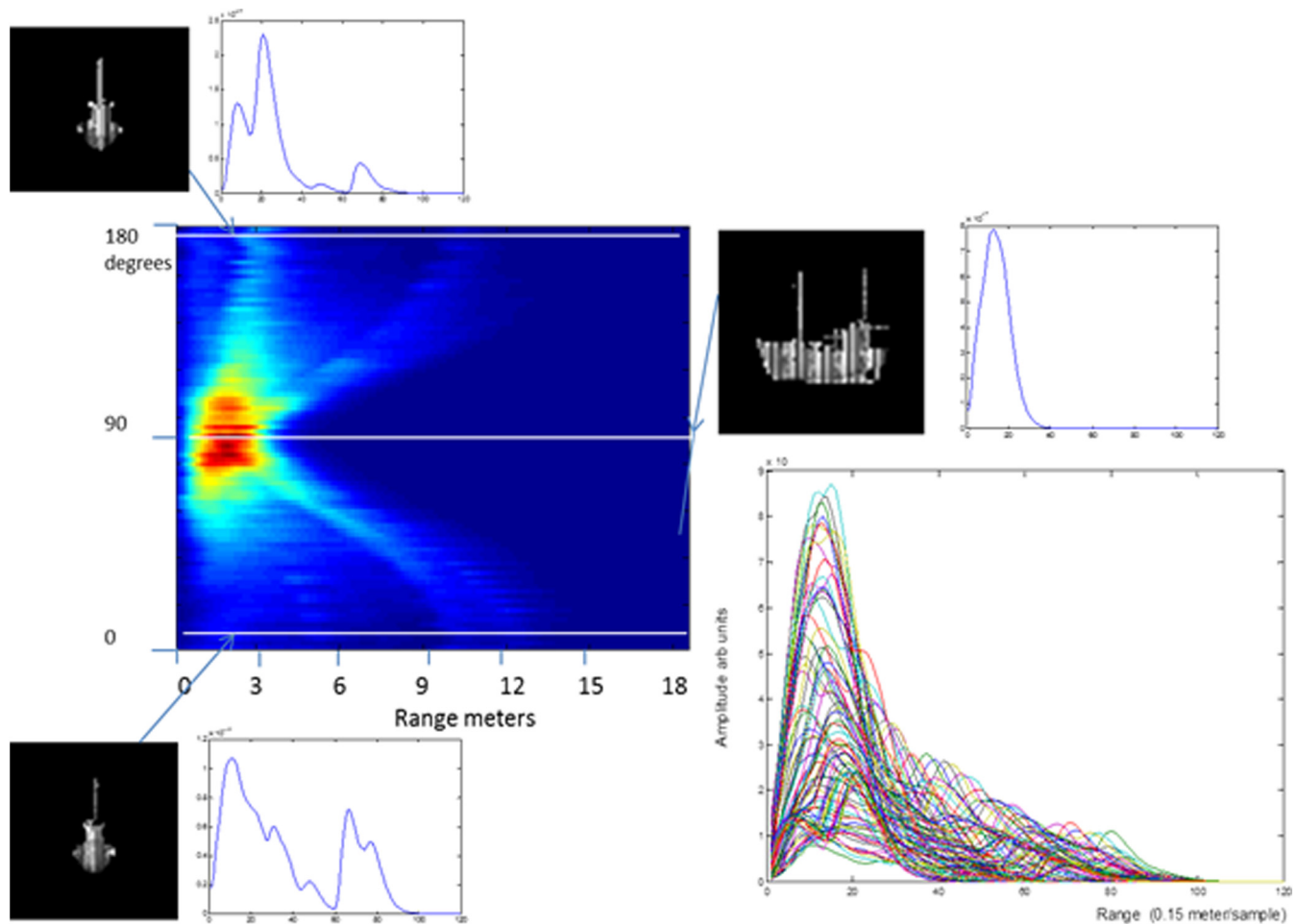


**Fig. 3** Examples of waveforms for the modeled fishing boat illustrated in Fig. 1. The middle figure is an intensity map of the waveform amplitude with an range in the x axis and the aspect angle  $\theta$  from 0 to 180 deg in steps of 2 deg where 0 deg if for an approaching frontal course. Around are examples of waveforms for  $\theta = 0, 90,$  and  $180$  deg. Below right are all the 90 waveforms from 0 to 180 deg. The assumed ladar system had a pulse width of 9 ns corresponding to a resolution of about 1.4 m and the length of the boat was set arbitrarily to 15 m. This pulse length does not resolve the structures in the side view at 90 deg.

over an area of  $400 \times 400 \text{ m}^2$ , sampled spatially with a 1-m resolution and a time resolution of 1 Hz for duration of 3 s. The reflection model of the sea surface follows that of Tratt et al.<sup>21</sup> The sensor height was assumed to be 15 m above sea level, which corresponds to a maximum viewing range to the surface of 14 km. Since the ranges studied were shorter (3 to 8 km) we omitted the effect of the earth's curvature. The turbulence was assumed to be constant with height. The simulations did not account for diedron or tredron effects from the superstructures.

### 3 Simulation of Range Profiles—Some Basic Investigations

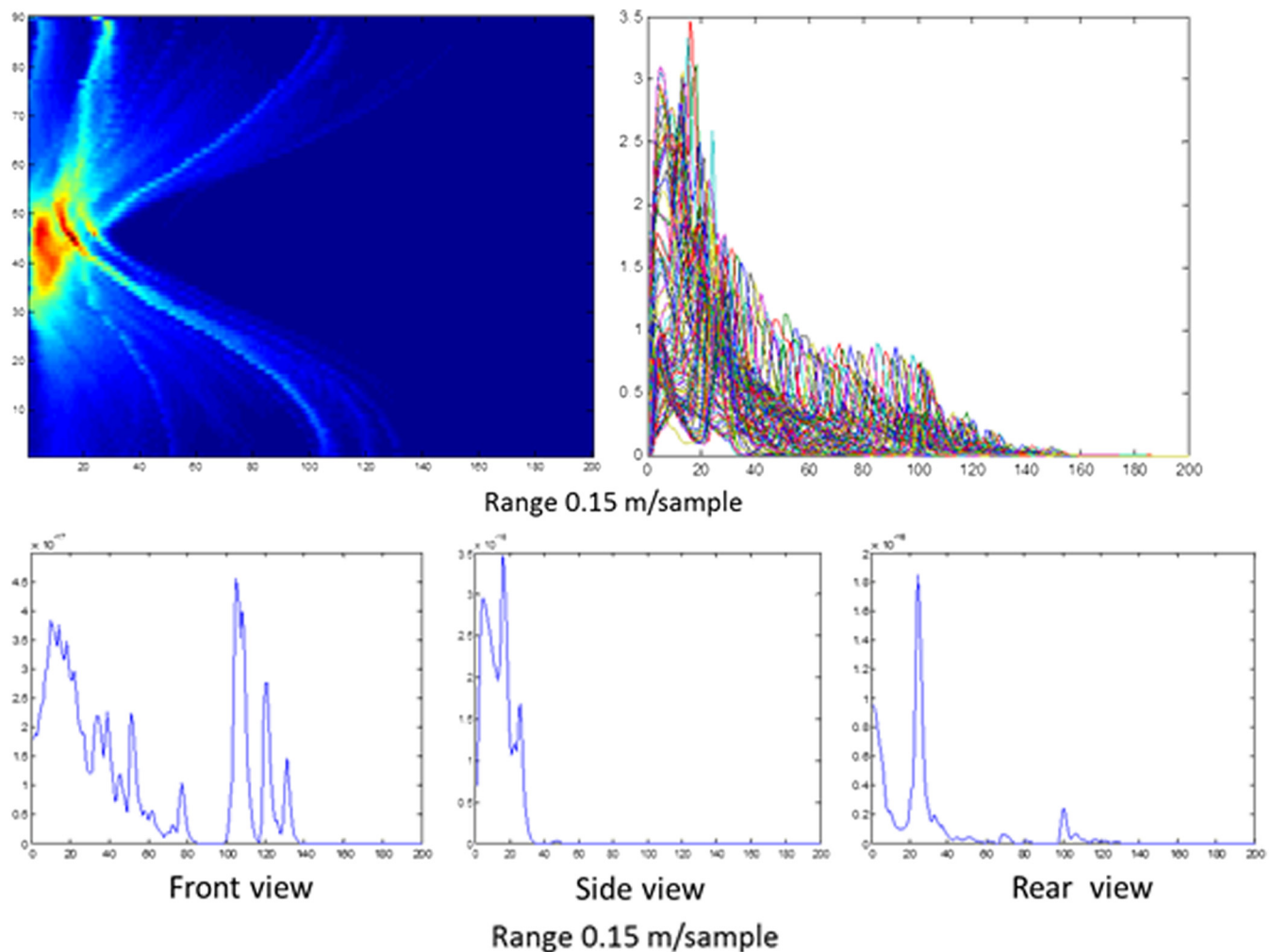
Figure 2 shows a toy model and a corresponding simplified 3-D model of a fishing boat used for simulation and measurements.

Figure 3 shows examples of a waveforms generated by a typical ordinary range finder with a pulse length full wave half maximum (FWHM = 9 ns) looking at the model of the fishing boat with an assumed length of 15 m. The range was assumed to be 2 km to ensure high SNR and the beam cross section was assumed to be Gaussian with a half width of 10 mrad. The receiver FOV matched the beam and the transverse resolution on the receiver waveform

calculations was set to be  $32 \times 32$  “angular pixels” within the FOV. In Fig. 2, examples of waveforms for  $\theta = 0, 90,$  and  $180 \text{ deg}$  are shown together with a range signature chart with a color intensity image of all waveforms from 0 (straight ahead) to  $180 \text{ deg}$  (from behind) in steps of 2 deg. The assumed lidar system had a pulse width of 9 ns which corresponds to a resolution of about 1.4 m and the length of the boat was set arbitrarily to 15 m. This pulse length does not resolve the structures in the 90 deg.

To study the full potential of high resolution imaging, we changed the laser pulse width and associated detector bandwidth to 3 ns and scaled up the boat length to 24 m, which in total corresponds to an increase in range resolution by a factor of 5. The result is shown in Fig. 4 and reveals many more details and structure in the waveforms as expected. The side view will, in this case, easily show the small range changes due to reflection from the hull and the cabin and from other structures on the ship.

The slope of the boat itself is less than the wave slope due to the length of the ship covering a good part of the wavelength and due to the inertia of the ship. To get an idea on how much the laser range profile changes, we let the fishing boat tip  $\pm 10 \text{ deg}$ . Figure 5 illustrates the result. The change can be rather large as some of the structure will have a different visibility for the different slopes.



**Fig. 4** The same as Fig. 3 but with an increased resolution by a factor of 5 (pulse length 3 ns and 24-m boat length). The signature will in this case contain many more details as expected.

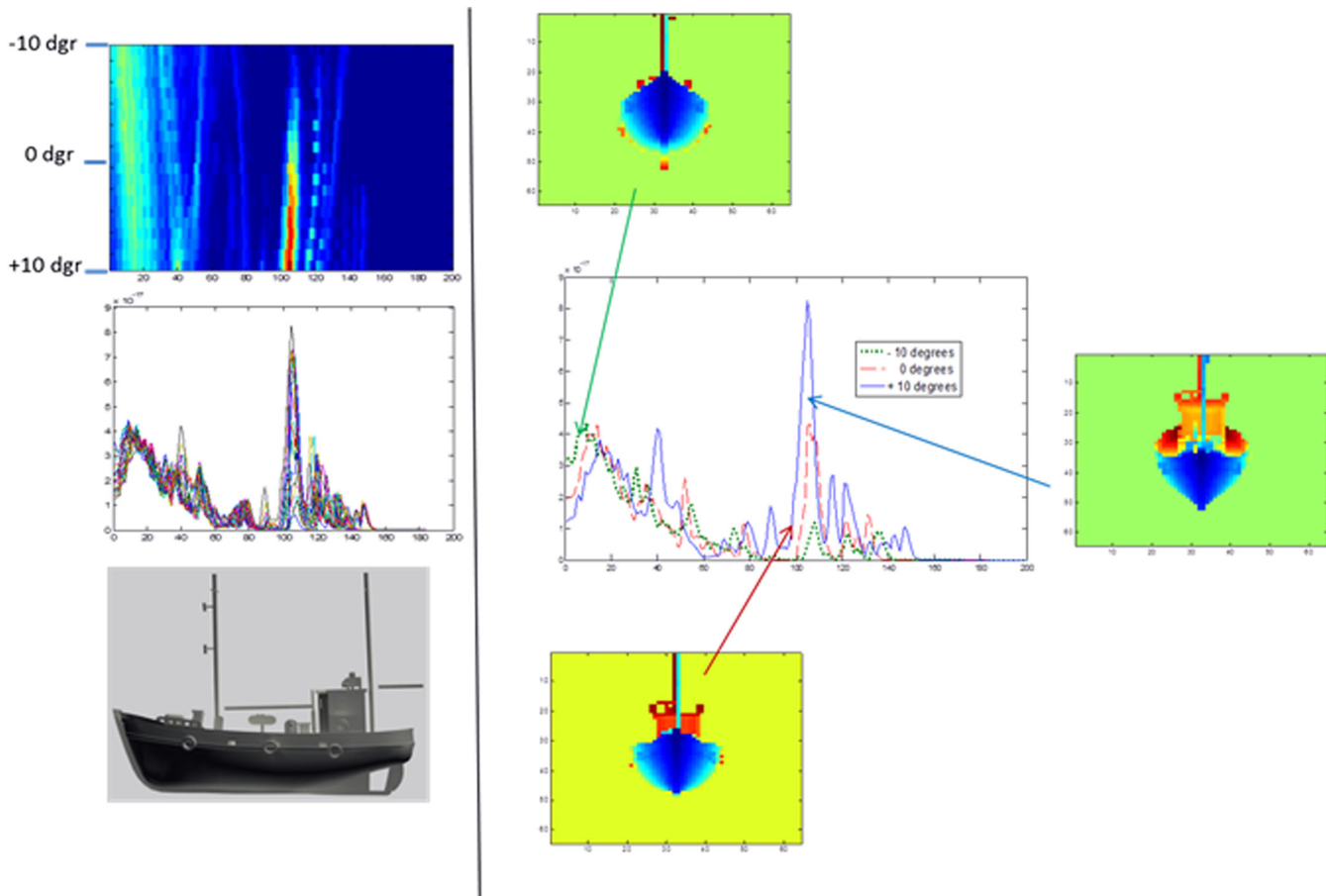


**Fig. 5** Illustration of the change in range profile in the front perspective when the boat is tipped  $\pm 10$  deg. The change can be rather large as some of the structure will have a different visibility for the different slopes.

The combined effect of course and slope on the laser range profile is illustrated in Fig. 6. If we limit ourselves to an approaching fishing boat with a course  $\theta = 0$  deg denoting straight toward the observer we can see that up to rather high deviating courses (60 deg chosen as maximum here in this example) the main features of the range profiles are conserved although the range between the features are “compressed” by  $\cos(\theta)$ . This is clearly illustrated in the lower part of Fig. 6 where we have corrected the 0 course range profile with the  $\cos(\theta)$  factor and compared with the corresponding profiles for the course  $\theta$ .

Figure 7 shows the high correlation between the profiles from different courses and different tip angles. In the right part, we have plotted the positions of the four highest peaks in the profile for different tip angles and courses [including the  $\cos(\theta)$  correction factor]. Knowing the course (from radar or tracking EO sensors) the recognition of the ship from the range profile seems attractive. It might even be that the reverse is possible, i.e., if the profile or ship type is known beforehand the course might be rapidly estimated within the uncertainty of the “sign,”  $\pm\theta$ .

#### 4 Measurements on Model Targets

In order to further study the potential of laser range profiling, we have conducted some laboratory experiments using single photon time correlated single photon counting (TCSPC),

which enables very high range resolution on the order or millimeter to centimeter. An overview of the TCSPC work at FOI was recently presented at SPIE.<sup>22</sup> This allowed us to use small toy models of ships to study range profiling and convert the results to real targets and systems by scaling about a factor of 10 to 100 in size. Our laboratory TCSPC lidar system had a time response of 54 ps corresponding to a range resolution of 0.8 cm. Realistic range resolution from conventional high resolution direct detection range finders of laser radars is in the region 0.2 to 1 m, which correspond to scale factors between 25 and 125. Figure 8 shows examples from the measurements using the 43-cm long fishing boat as a target. Left is an example of the observed waveform looking straight at the fore of the boat, middle and range profile for 341 deg in steps of 1 deg. Right is a tomographic image obtained by using the Radon transform to reconstruct the plane shape of the boat.<sup>23</sup> The measurement range in the laboratory was about 40 m and the beam covered the whole FOV of the receiver, which was 10.2 mrad ( $1/e^2$ ) corresponding of 40 cm at the target.

Figures 9 and 10 show examples of range profiles from a model row-boat (30 cm in length) with and without people onboard. In Fig. 11, we have tested a tip of 6 deg along the long side and registered the intensity signatures. As can be seen from these data as well as the modeling experiments in the previous section, the main features remain after tipping the boat at the moderate angles to be expected at sea.

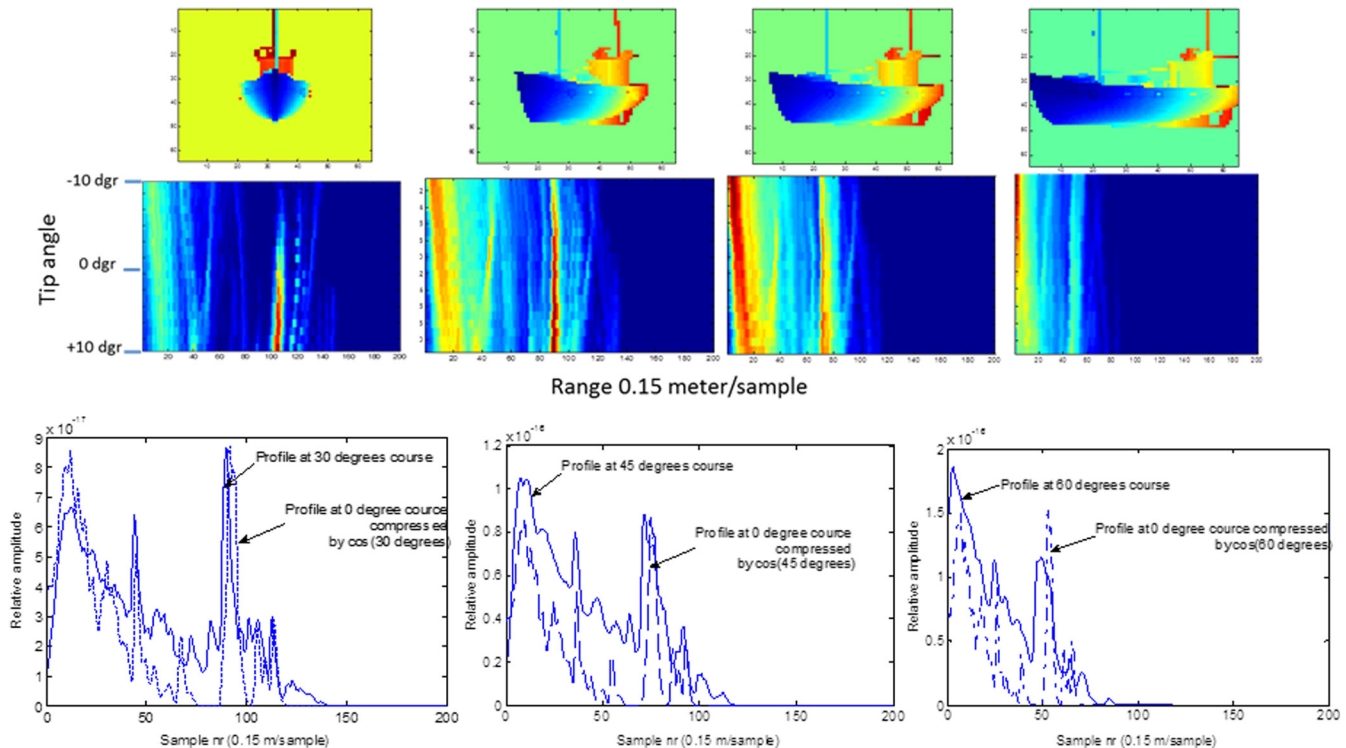


**Fig. 6** The top row shows the range profiles for the fishing boat observed at different courses and tip angles. The bottom row is a comparison of different profiles at courses  $\theta = 30, 45,$  and  $60$  deg with the  $\cos(\theta)$  compensated range profile at  $\theta = 0$ .

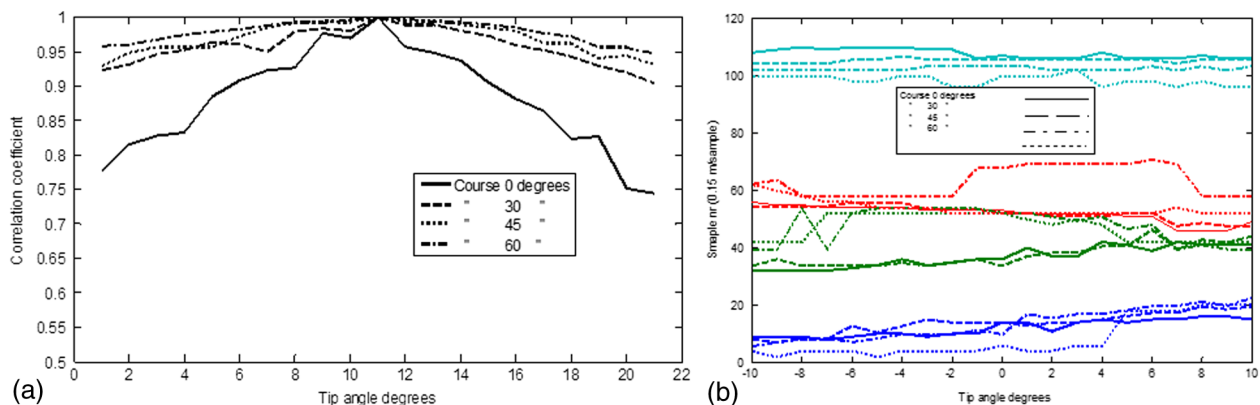


**Fig. 7** (a) Correlation for the range profiles at different tip angles and for different courses. The correlations are high especially at oblique courses. (b) The positions of the 4 highest peaks in the profile for different tip angles and courses [including the  $\cos(\theta)$  correction factor].

One problem in comparing measurements with models is the lack of information about the angular reflectivity of all structures and parts of the ship. In our models, we have simply assumed an equal diffuse reflectivity for the whole ship, which makes a detailed comparison with measurements difficult. On the other hand in a real situation where the available information about a ship may be deduced from photos only and the reflectivity information at the laser wavelength is very hard to know in advance so the comparison of models and measurements become motivated from several aspects. Parallel to building a library from geometry, the library may also contain real measurements from targets of opportunity from a few aspect angles only. A model effort to use geometry plus existing range profiles and deduce profiles in other directions is also motivated.

Figure 12 shows an example of comparisons between modeled and measured waveforms from the fishing boat at 0 (approaching) and 90 deg course and with tip angle 0 deg. As seen the correspondence is rather good, at least for the positing of the main peaks.

## 5 Extended Simulations

After the preliminary investigations described above, we extended the model boat library by 15 different digital boat models acquired from a public site on the Internet.<sup>24</sup> Some of them needed some corrections using scaling, translation and rotation. All surfaces on all boats were modeled using the same material description with a diffuse as well as a specular component. A generalized form of the BRDF is written

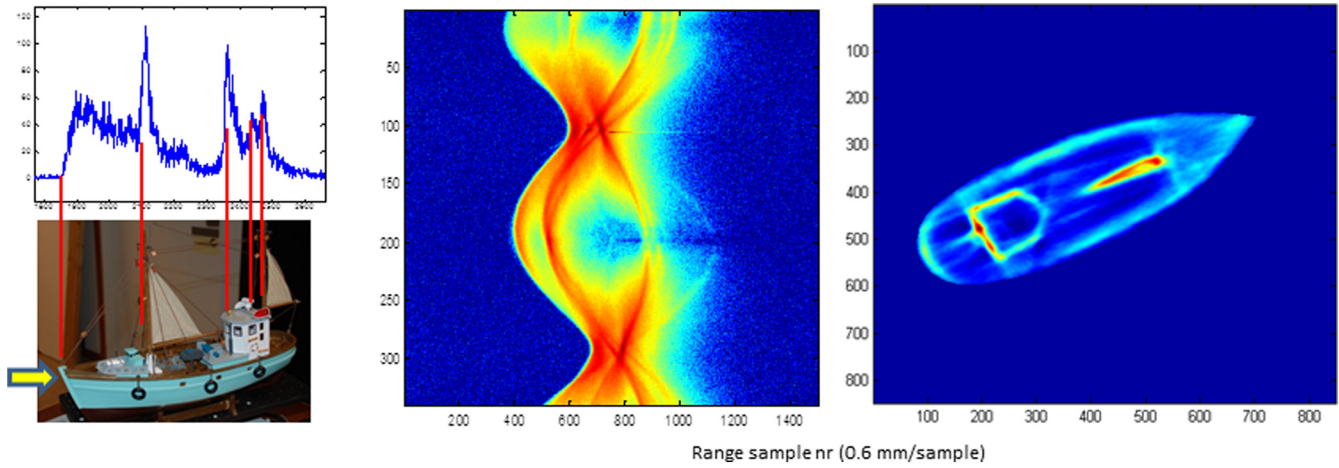


Fig. 8 Tomographic image of boat.

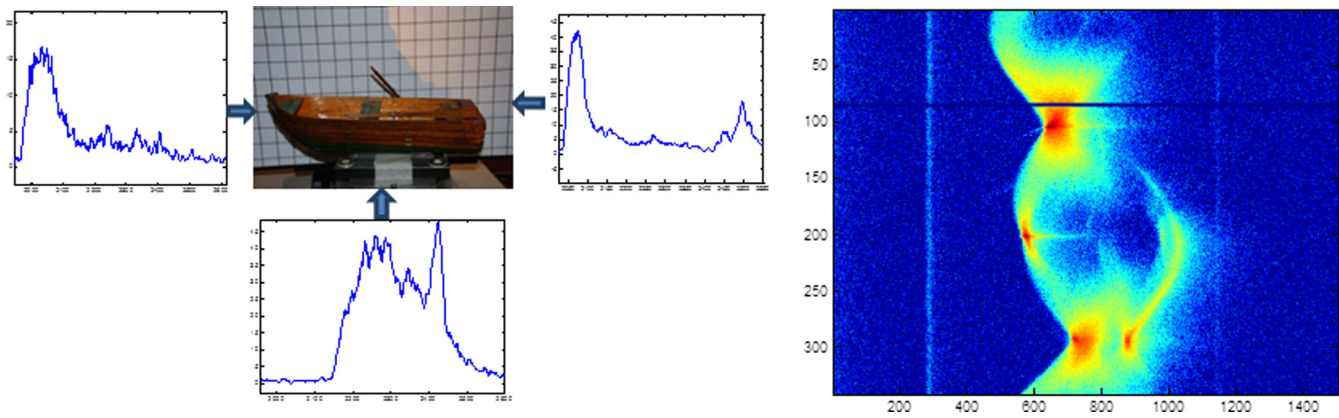


Fig. 9 Example of measured waveforms from a small row-boat and the intensity signature of 341 waveforms.

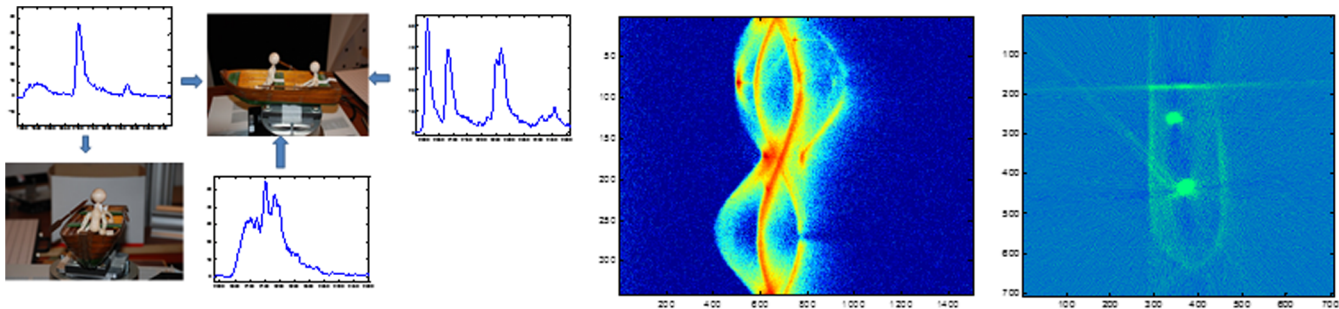


Fig. 10 Example of waveforms with two persons in the boat. Right the tomographic image based on the data in the middle.

$$BRDF_{tot} = BRDF_{diff} + BRDF_{spec}$$

$$= A \cos(\theta)^m + [B / \cos(\theta)^6] \times \exp\left[-\frac{\tan(\theta)^2}{s^2}\right]. \quad (1)$$

In the simulation, we used  $A = 1$  m,  $B = 0.2$  m, and  $s = 0.1$ . Figure 13 shows thumbnails of the boats and Table 1 lists the boat names and their characteristic dimensions.

### 6 Parameters Used in the Main Simulation

The simulation derives 1-D, 2-D, and 3-D information from the target illuminated with a short pulse eye safe laser at

$1.5 \mu\text{m}$ . The 1-D refers to the range profile, 2-D to the intensity image summed over the whole time gate placed around the target, with a total gate time of 200 ns, corresponding to 30 m. The 3-D data set refers to the 3-D target data as detected by a pixel array. For each pixel, peak detection was performed to detect the position and the intensity of highest peak. Environmental parameters were limited to variations of the wave height given by the wind and different atmospheric turbulence values. Other laser system parameter variations like pulse energy and receiver size are affecting the SNR and are easily simulated by changing the SNR of a given scene simulation.

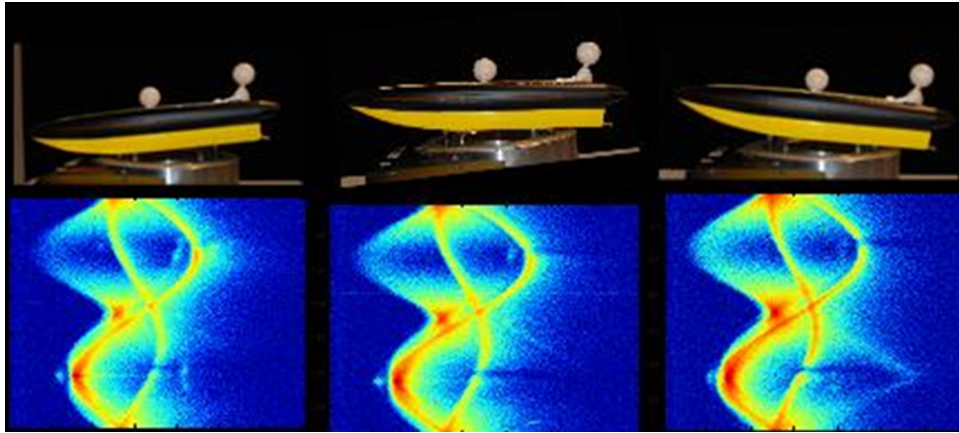


**Fig. 11** Tipping the row boat  $\pm 6$  deg and the associated range profiles for 341 angles.

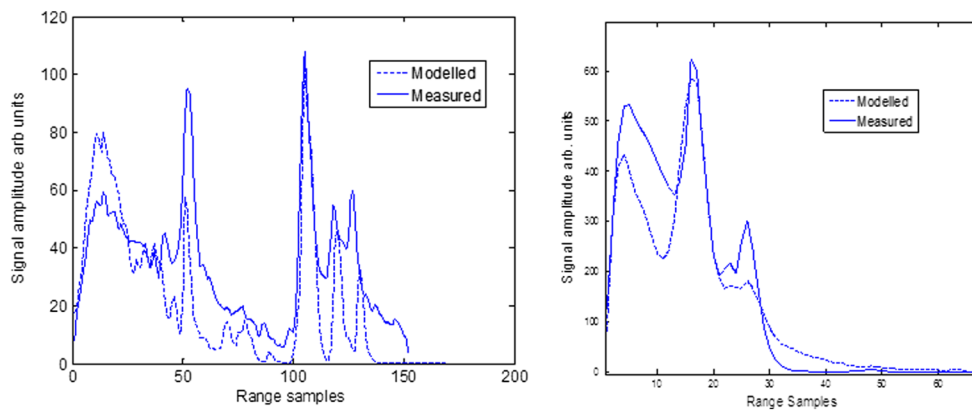


**Fig. 12** Comparison between measured and modeled range profiles of the fishing boat. (a) Boat with course 0 deg, 0 tip angle. (b) Side view at 90 deg.

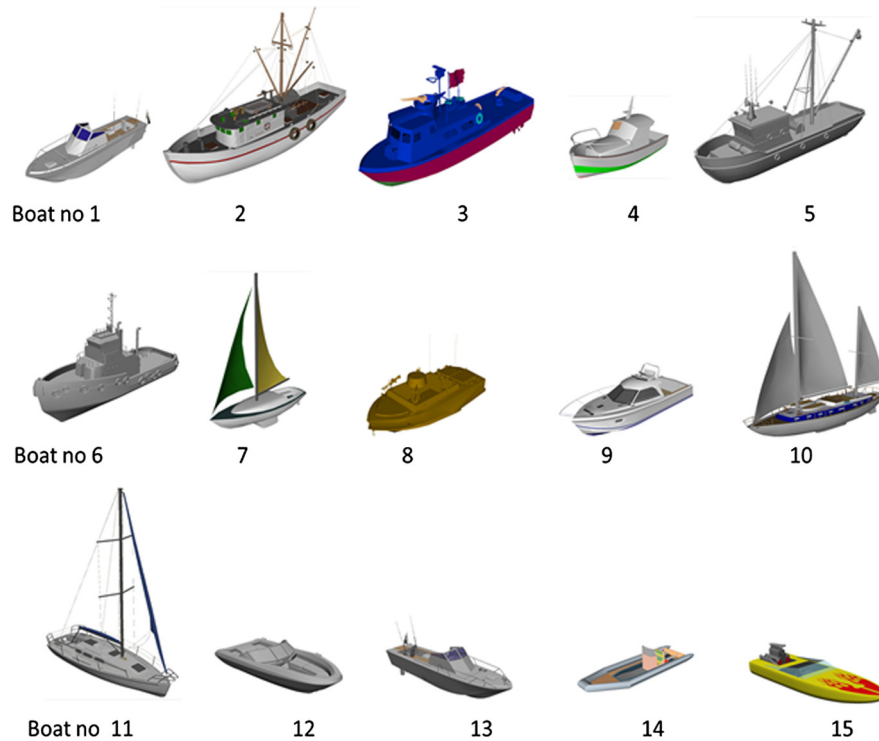


**Fig. 13** The digital boat models used in this study. They are all downloaded from a public website, <http://www.3dcadbrowser.com/download.aspx?3dmodel=7024>.

**Table 1** The name of the boats and their characteristic dimensions.

Boat name	Boat number	Dimension meters		
		L	W	H
677_Fishing_Boat_Wahoo	1	9,21	2,21	2,72
982_Shrimp_Boat	2	16,77	6,06	9,67
3201_U_S_Navy_Swift_Patrol_Boat	3	15,91	4,27	5,36
6996_Boat_Fishing	4	6,13	2,40	2,69
47299_Fishing_Boat	5	15,23	3,80	9,3
53338_Sydney_Tug_Boat	6	15,62	5,31	8,45
2056_Sailboat	7	8,13	2,89	9,75
3332_LSSC	8	8,67	3,43	3,82
5086_Boat	9	6,55	1,88	2,42
11851_Sailboat	10	17,91	4,72	20,57
45476_Sailboat_Yacht	11	7,51	2,69	9,34
47118_Lancha	12	6,26	2,51	0,97
57561_Lancha_Pesca_Deportiva	13	7,26	1,74	225
7024_Rigid_Inflatable_Boat_RIB	14	4,37	1,49	0,76
47148_Speed_Boat	15	3,47	1,49	0,5906

In the simulation, we assume a laser with a 3-ns pulse length (FWHM), a pulse energy of 50 mJ, a beam divergence (at  $e^{-2}$  intensity) of 10 mrad and a repetition rate of 10 Hz. The assumed laser wavelength was 1.5  $\mu\text{m}$ . The visibility was set to 20 km, which implied an atmospheric attenuation factor of 0.051/km at the laser wavelength. The detector was assumed to have  $128 \times 128$  pixels with 20- $\mu\text{m}$  pixel size and a noise equivalent power (NEP) = 3 nW per pixel. The pixel IFOV = 20  $\mu\text{rad}$ . This implies 1 total FOV =  $120 \times 0.02 = 2.4$  mrad. The detector bandwidth was assumed to be 300 MHz. Summing up the signals from all pixels enables us to simulate a range profiling system with one detector instead of the array. For this case, a bandwidth of 300 MHz is state of the art.

The atmospheric turbulence was varied assuming a homogeneous turbulence constant  $C_n^2$  from  $10^{-15}$  to  $5 \times 10^{-13} \text{ m}^{-2/3}$ . Three wave height conditions were simulated corresponding to wind velocities between 2, 5, and 10 m/s. The wind direction was assumed according to Fig. 1.

## 7 Analysis of the Range Profiles

### 7.1 Range Profiles at 0 deg Course (Direct Approach)

We started by keeping the turbulence and the water height at low values. Figure 14 shows example of simulation output from a fishing boat (no. 5 in Table 1) illuminated at 8 and 5 km, respectively. The output in this case shows the intensity image as detected without and with detector noise, respectively. The corresponding range profiles (waveforms) are shown beneath each image. The sampling unit in time is

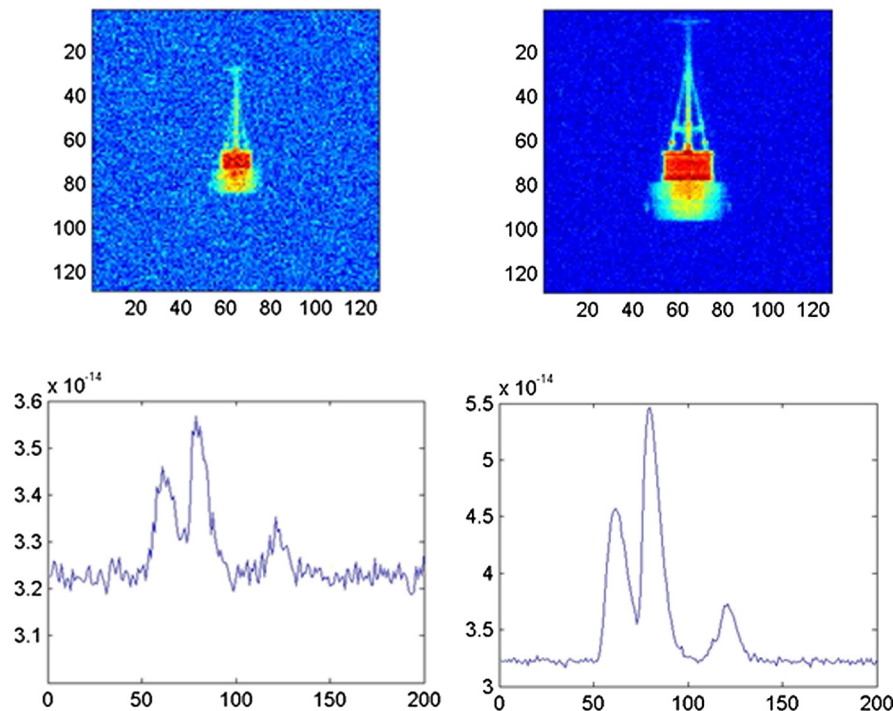


**Fig. 14** (a) The two intensity images of a fishing boat (no. 5 in Table 1) as observed at 8 km. Below the corresponding range waveform sampled at 1 ns/unit of the return energy (in joules). (b) The corresponding at 5-km range.

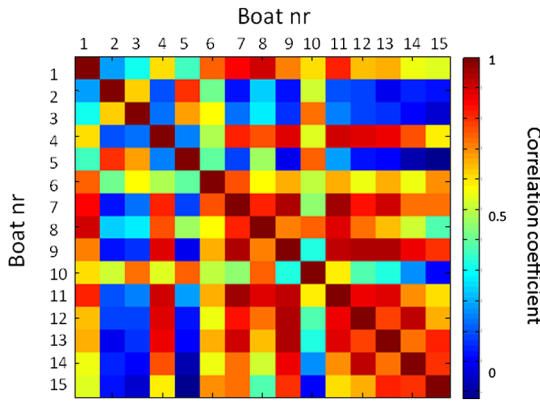


**Fig. 15** The correlation matrix between boat profiles with no detector noise. The separation capability between the larger boat (no. 1 to 5) is better than for the smaller boats (especially boats 10 to 15). The value of the correlation coefficient is color coded as shown by the color bar (0 to 1).

1 ns corresponding to a range step of 15 cm. We assume all boats to have a course directly toward the sensor.

As a measure of the separation capability of the different waveforms from 15 different boats, we calculated the correlation matrix (Fig. 15) for the correlation between the noise free waveforms from 8-km range. We can see the correlation coefficient is rather high (indicating low separation) between the boat numbers 10 and 15, which correspond to rather small boats (cf. Fig. 1) with often unresolved longitudinal features. The same holds for boat numbers 7 to 9. The separation is better between boats 1 and 5, which are larger and thus show more resolved features in the length direction. Figure 16 shows the correlation matrix between waveforms including noise, observed at 8, 5, and 3 km. For shorter ranges the SNR is increasing (from a relative low value at 8 km), which is favoring the separation between the different waveforms.

We also performed peak detection to correlate with the geometry of the boats. The peaks were assumed to

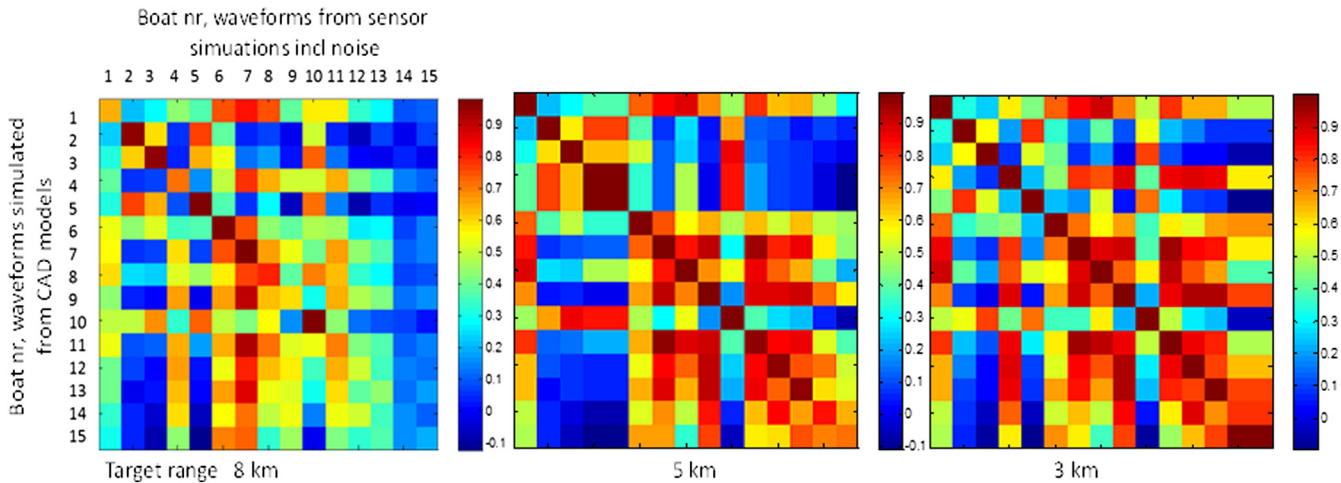


**Fig. 16** The correlation matrix between boat profiles with no detector noise and those from the simulated sensor including noise. The separation capability is increasing with increasing signal-to-noise ratio (shorter ranges).

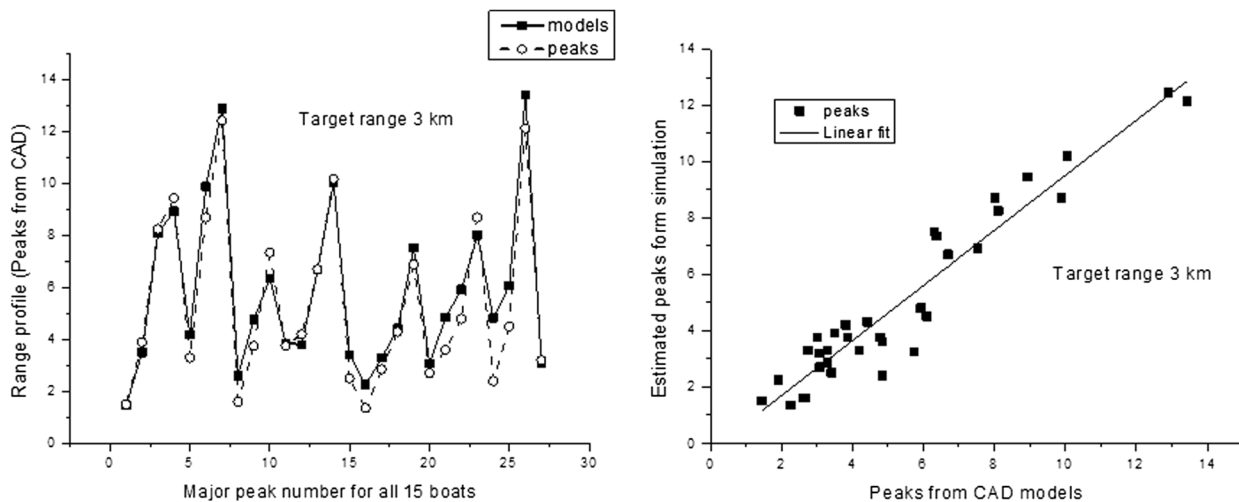


**Fig. 17** (a) A comparison between the peaks “extracted by hand” from the CAD models and those obtained from the simulated waveforms. Target range 3 km and low turbulence ( $C_n^2 = 10^{-15} \text{ m}^{-2/3}$ ). The peaks originate from the major peaks from all the 15 boats at a range of 3 km. (b) A regression line between the simulated data and that derived from the CAD model directly. The correlation coefficient was 0.96.

approximately correspond to the central portion of features, such as the wind shield, cabin, or mast and were extracted “by hand” from the computer aided design (CAD) models. The peak detection data were obtained with a simple peak finding algorithm. For the noisy data (at 8-km range), we filtered the waveform with a 10 point moving average. Figure 17 shows a comparison of the main peaks detected from the simulated waveforms and the peak positions derived directly from the CAD models. The correspondence is good with a correlation coefficient of 0.96. The data used in Fig. 17 were obtained from the 3-km target range. For an 8-km range for which the SNR was rather small, the corresponding peaks did not always match those derived directly from the CAD models.

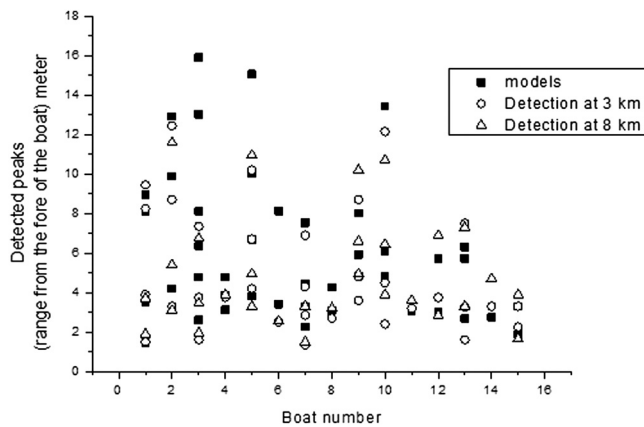


**Fig. 18** Detected peaks for each boat derived directly from the CAD models as well as from simulated waveforms for the boats at 3 and 8 km range.

In several cases, the peaks were missing in the data derived from the waveforms when compared with the peaks from the model. This may have several reasons, one is that the feature in the CAD model may have a low geometric cross section or has a slope, which leads to pulse stretching. Another reason is erroneous detection due to noise, which is present especially for the 8-km data. Figure 18 compares the detected peaks for each boat derived directly from the CAD models as well as from simulated waveforms for the boats at 3- and 8-km range. For shorter distances, the correspondence is rather good but peaks at larger depth could be missed due to low SNR and that the features associated with the peaks are occluded.

### 7.2 Influence of Beam Jitter on Range Profiles

Beam jitter is a reality for lidar systems. The aim point of the beam may stochastically vary from pulse to pulse due to system or turbulence induced jitter. Figure 19 illustrated three snapshots for a beam jitter with a rms jitter equal to 1/3 of the sensor FOV, as seen from this figure, and also illustrated in the following. In Fig. 20 the peak position is maintained but the relative amplitude among the peaks are changed.

We conclude that beam jitter will not change the peak positions but may alter the relative amplitude distribution of the peaks.

### 7.3 Influence of Waves on Range Profiles

We have investigated the boats moving in different sea states. We limited ourselves to wind velocities of 2, 5, and 10 m/s. We omitted higher sea states because these will generate foam and will wet the boat surfaces, something we are not simulating at the moment. Wet surfaces,

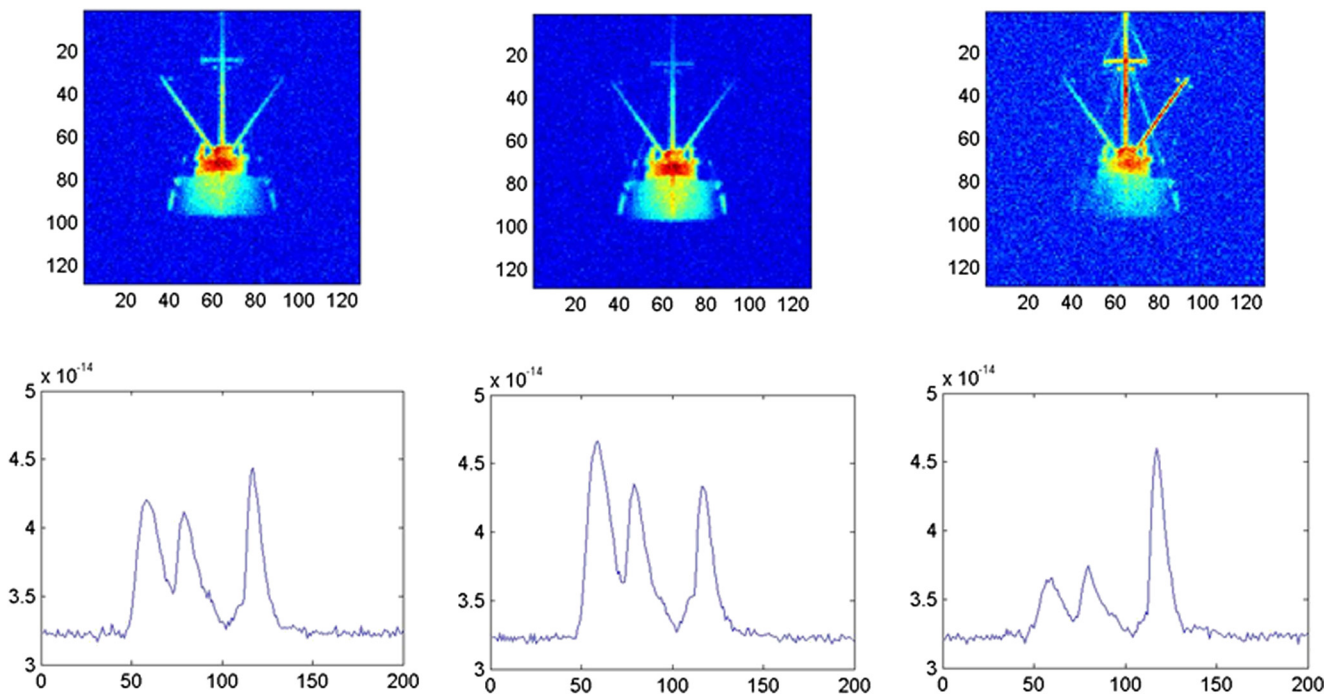


**Fig. 19** Illustration of the effect of large beam jitter with an rms value equal to 1/3 of the field-of-view (FOV). The peak positions remain unchanged but not the mutual peak amplitudes.

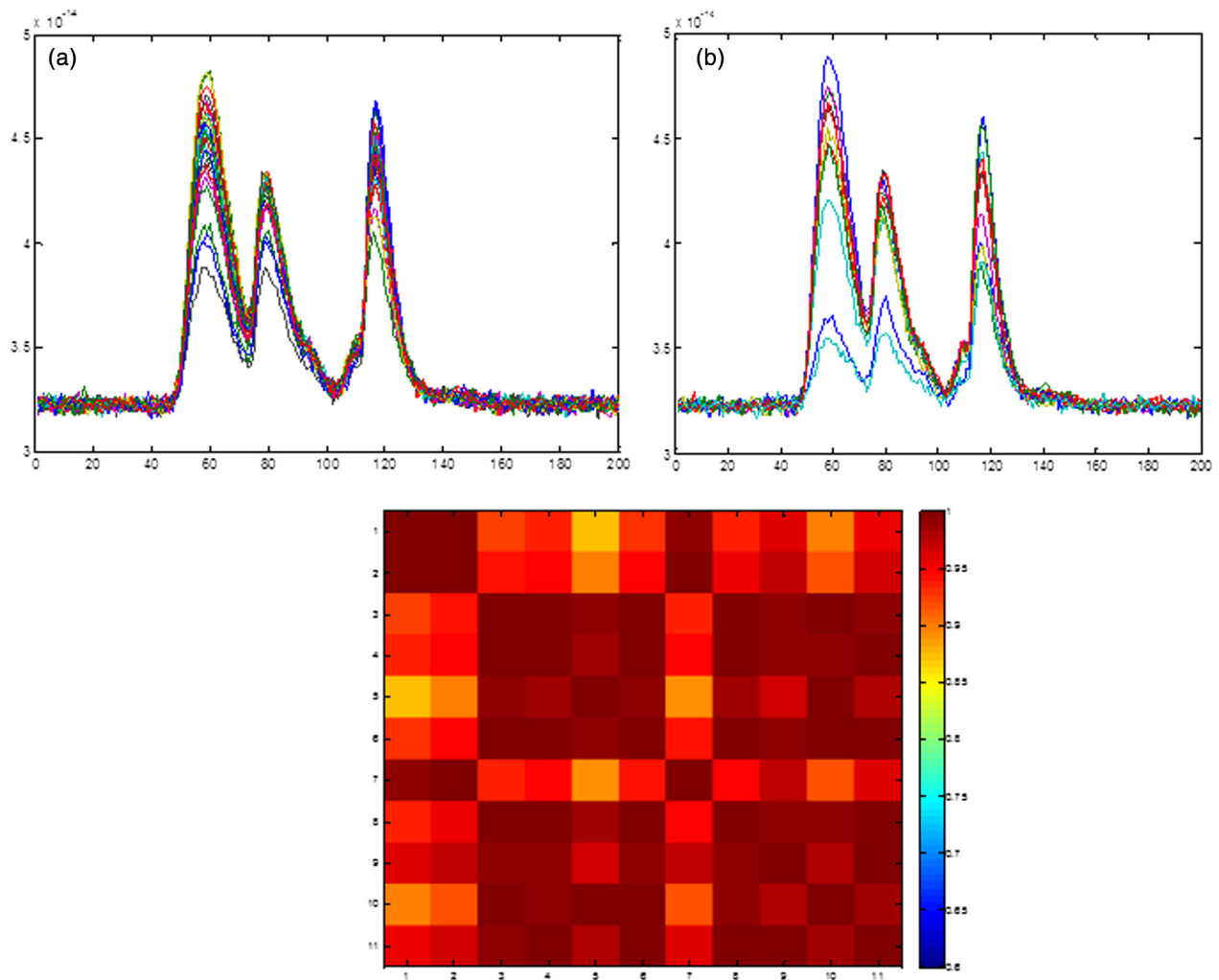


**Fig. 20** A series of waveforms for different beam jitter. (a) The rms jitter is assumed to be  $=1/10$  of the FOV or  $0.256$  mrad. (b) The corresponding with a beam jitter  $= 1/3$  FOV  $= 0.85$  mrad. Above the shape of waveforms and below the corresponding correlation matrix between the different waveforms. Note the color bar span from  $0.8$  to  $1$  for the correlation coefficient.

however, are of high importance since the water reflectivity is low at  $1.5\text{-}\mu\text{m}$  wavelength. The water reflection from the sea was so low that, in practice, we could omit water backscatter when analyzing the waveforms. For a wind velocity of  $5$  m/s the wave height may reach  $0.7$  to  $0.8$  m and for  $10$  m/s the wave height may reach  $2$  m assuming a long fetch.

Figures 21 and 22 illustrate the boat movement and waveforms for a wind velocity of  $5$  and  $10$  m/s, respectively. Figure 21 shows a series of sampled waveforms for a wavy sea surface assuming a wind velocity of  $10$  m/s. The boat movement affects the waveform shapes so the magnitude of the peaks is changed as well as the generation of new peaks which come and go with the movement. The time difference between the sampled waveforms is  $1$  s. Figure 22 shows two time sequences for wind velocities at  $5$  and  $10$  m/s during of  $2.5$  and  $3$  s, which correspond to  $25$  and  $30$  pulses respectively for the  $10\text{-Hz}$  laser. The left diagrams show the color coded waveform intensity versus time (pulse no.) and the middle pictures illustrate the different waveforms. To the right the correlation matrices between the waveforms are shown. Note the different color scales indicating that the  $5\text{-m/s}$  case only leads to a decorrelation

down to  $0.98$  while the corresponding decorrelation for the  $10\text{-m/s}$  case has values down to  $0.6$ . The correlation matrix has a lot of information about the specific movement of the boat in the sea which might help the classification.

#### 7.4 Influence of Turbulence on the Range Profiles

The turbulence introduces blur and beam scintillation that is a stochastic re-distribution of the intensity within the beam. It will also introduce a small beam wander. Figure 23 shows examples of waveforms for increasing turbulence for a boat at  $8\text{-km}$  range. Note the increasing blur in the intensity image and the change in relative amplitude among the peaks. The peak position is fairly stable. By investigating several boats we typically find, after using a peak finding algorithm and some smoothing, that the error in the peak positions typically was  $<2$  samples or  $0.3$  m.

In the example, from Fig. 23, we find that the correlation coefficients between the optical waveform without turbulence and noise and the waveforms in turbulence were  $0.95$ ,  $0.92$ ,  $0.82$ , and  $0.78$ , respectively. The correlation is slowly degrading with turbulence as should be expected. For the same boat at  $5$  km the corresponding correlation

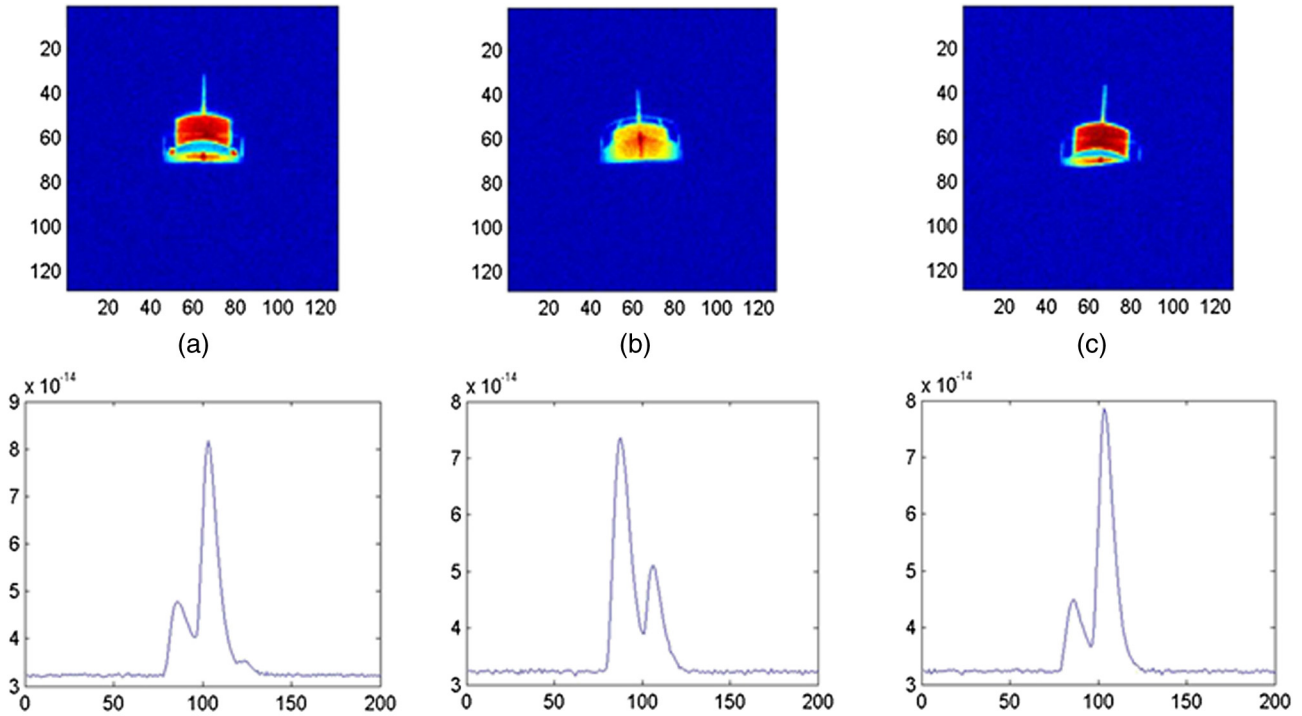


**Fig. 21** Examples of different waveforms and boat aspects during a sea state corresponding to a wind velocity of 10 m/s. The time difference between the sampled waveforms is 1 s. Boat no. 2 at a range of 3 km.

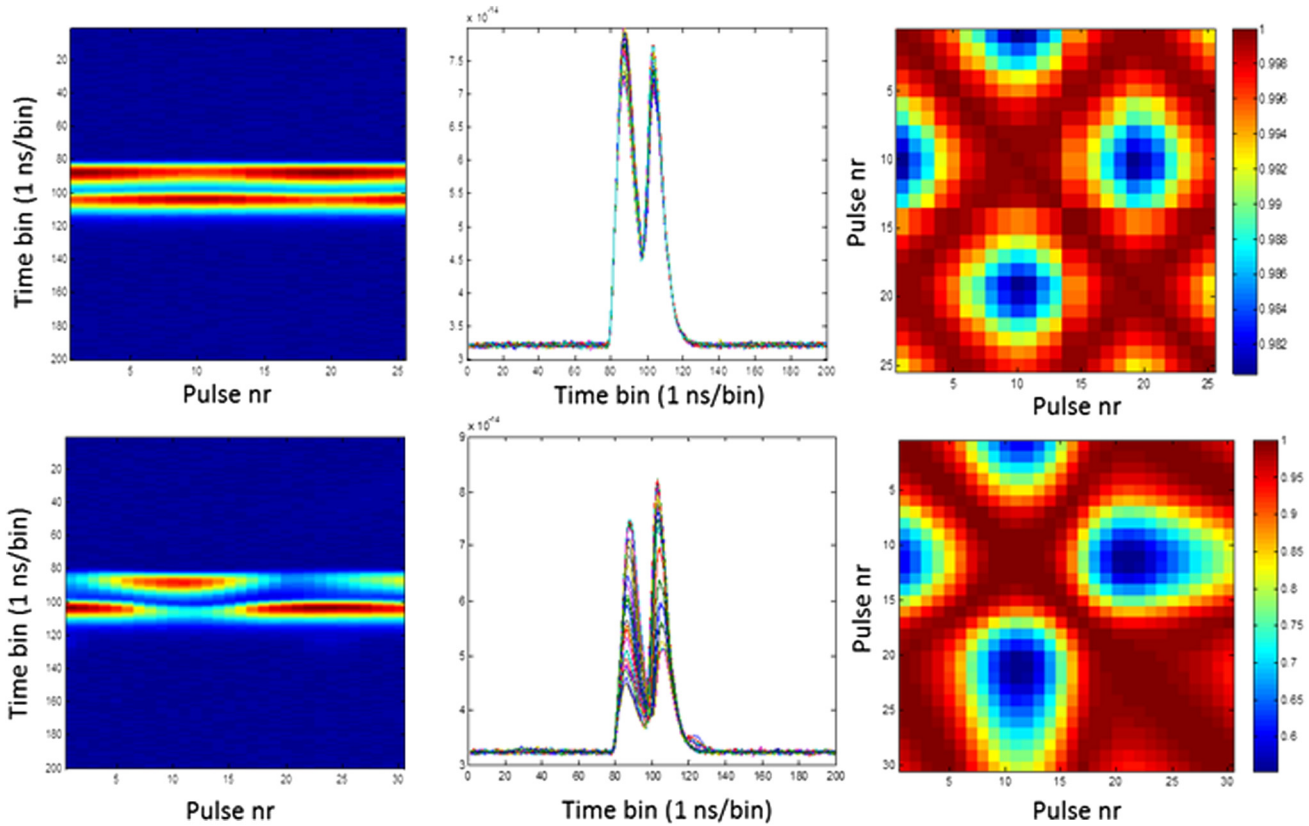


**Fig. 22** (a) The time history of the intensity of the waveforms in different sea states. The laser pulse repetition was 10 Hz. (b) The variation of waveform shape is shown and (c) the correlation matrices between the waveforms for the different wind cases. Note the different span of correlation coefficient values which for the 5-m/s wind was 0.98 to 1 (top row) and for the 10-m/s case, 0.6 to 1 (bottom row). The pattern of the color-coded correlation matrix might reveal how the boat is behaving at sea which can support the classification process.

values were 0.9970, 0.9985, 0.9756, and 0.9249, respectively and for 3 km 1, 0.9997, 0.9903, and 0.9784. The turbulence has thus a minor influence on the waveform shape especially at higher SNR occurring at closer ranges.

## 8 2-D and 3-D Data Extraction

By taking all pixels into account from the assumed detector array, we can form 2-D images of boats (cf. Fig. 23 for example). The detected points on the target will also allow estimation of the boats' transverse dimensions. This can be done by a rectangle estimator developed by Grönwall et al.<sup>25</sup> and is done and discussed in Ref. 26. The estimate of the width and height were quite sensitive to the range, which is probably connected to a higher SNR and more number of pixels at the shorter ranges. The accuracy of the width and height were typically on the order of 1 to 2 m, which at least enables separation of different classes of boats.

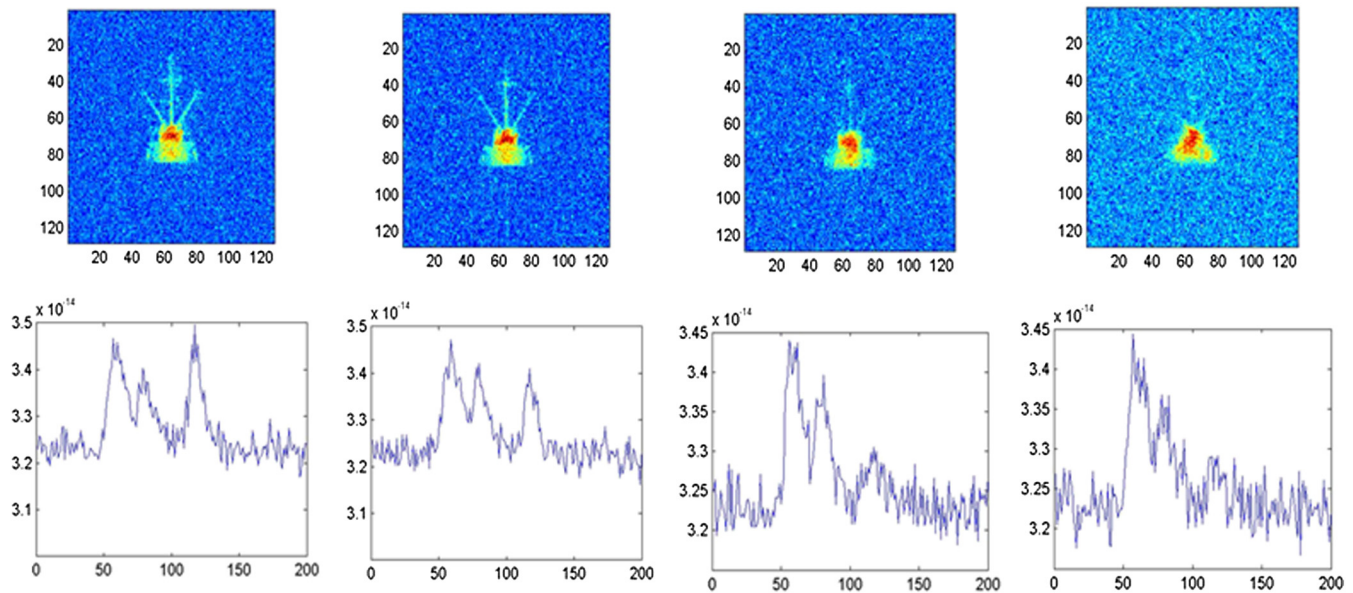


**Fig. 23** Examples of waveforms for increasing turbulence for boat no. 2 at 8-km range. Note the increasing blur in the intensity images and relative change in the peak amplitudes. The peak positions are relatively constant. The turbulence levels were from left to right  $C_n^2 = 10^{-15}$ ,  $10^{-14}$ ,  $10^{-13}$ , and  $5 \times 10^{-13} \text{ m}^{-2/3}$ , respectively.

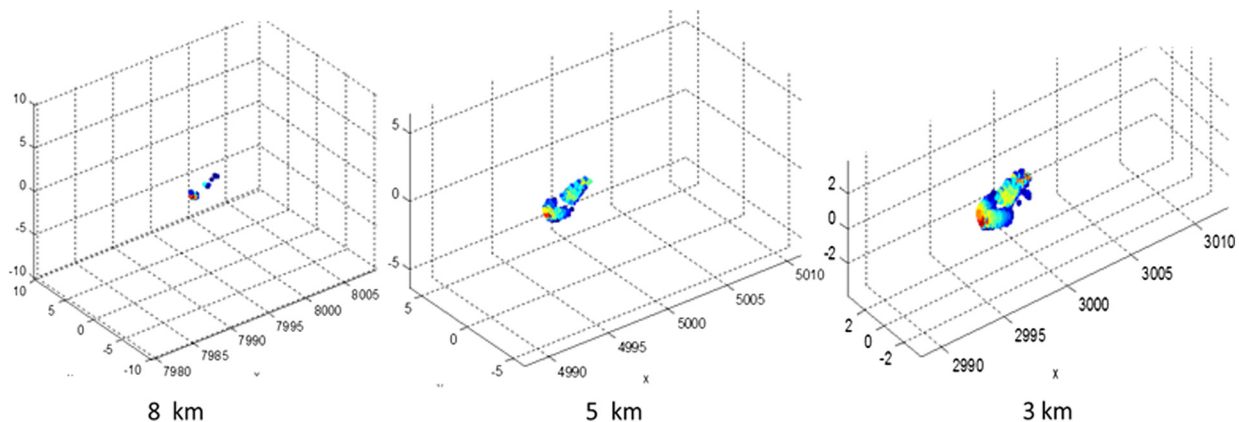


**Fig. 24** Example of detected 3-D point clouds for boat no. 9 approaching toward the sensor at different ranges.

Figure 24 illustrates the number of detected points for boat no. 9 as a function of range. As the pixel IFOV =  $20 \mu\text{rad}$ , we should estimate the theoretically maximum number of 3-D point/ $\text{m}^2$  cross-section area as 39, 100, and 277 for 8, 5, and 3 km, respectively. In reality, the number is smaller, especially for low SNR occurring at oblique incidence for the beam against a target surface.

A simplified 3-D target recognition technique based on rectangle estimation has been developed at FOI.<sup>25</sup> It was developed for ground vehicle recognition but has been used for land mine recognition as well. It involves estimating the size and orientation of a segmented object through simple geometrical assumptions and partitioning of the object into geometrical primitives (rectangles). The size and orientation estimates are then used to initialize a least-squares fitting procedure with a CAD model. While target/background segmentation directly in noisy 3-D data from cluttered scenes is quite error-prone, we should

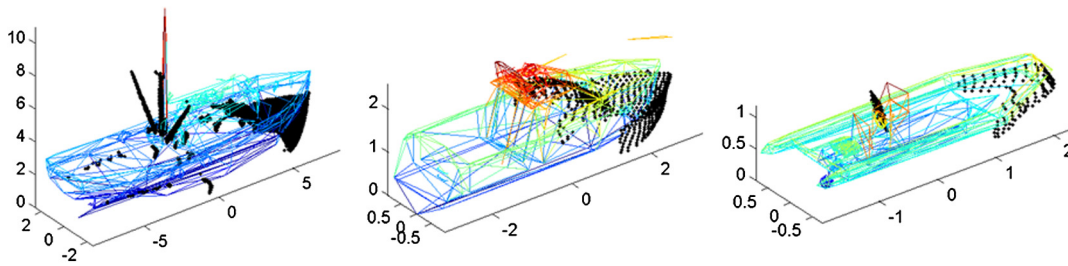


**Fig. 25** CAD matching with correct model for (a) boat 2, (b) 9, and (c) 14, target range 3 km. Number of target samples: 3402, 803, and 199, respectively.

use the fact that there are other sensor modalities (1-D and 2-D) that can be used to detect possible targets, i.e., provide the first steps of target/background segmentation. After target/background segmentation, the target dimensions are estimated by fitting a rectangle to the object data. The dimension estimates are used to select library models of corresponding dimensions. This means that only library models of relevant size are selected for CAD model matching, and this reduces the number of matches that need to be performed. Finally, the object data are fitted to the CAD model by iterative least-squares fitting. Examples of matching results are shown in Fig. 25.

## 9 Discussion and Concluding Remarks

In this article, we have simulated laser profiling and imaging of small surface vessels between 3- and 8-km range. The results clearly indicate the potential of using a laser to detect and classify these types of targets. This simulation has been made within a project at FOI,<sup>2</sup> which also will involve radar and passive IR/TV for having a robust solution to detect, classify, identify and track small boats at sea. The radar module is responsible for detection and positioning of target candidates and periodically estimates about directions and distances to the target candidates available on the computer network, thus cueing the other sensor modules. The EO sensor can in turn provide high-resolution profiles and images of the target candidates, making classification and/or identification of potential targets possible.

The profiling is assumed to be most important at long ranges where the target transverse resolution is limited. For the assumed laser and receiver parameters the range profiles from 8 km were rather noisy especially for the smallest vessels. Pulse integration during 1 to 3 s will improve the SNR and more accurate profiling data can be obtained. The correlation matrix was used as an indicator for the separability between the 15 boats. It showed that the separability was rather good for the 3- and 5-km range and more limited at 8-km range. The data at 8 and 5 km may be comparable if we increase the SNR at 8 km with a factor  $(8/5)^4$  or roughly 7. This would for example need a pulse integration of 49 pulses or to use a smaller beam and/or a larger telescope area. The beam divergence could be reduced to 3 mrad instead of 10 mrad, which would increase the SNO by more than a factor 9. The correspondence between detected peaks from the simulated waveforms and the peak locations derive from the CAD model showed a very good correlation (0.96) for the 3-km data and all boats. For the 8-km data, the main peak locations were also in good correspondence with the “true” values from the CAD models except for 3 cases where the peaks at larger depth were missed due

to low SNR and occlusion. We can also conclude that it would be valuable if the range resolution could be improved, for example using the TCSPC techniques.<sup>27</sup> The simple peak finding algorithm will also give larger range errors compared to other techniques such as constant fraction detection, Gauss fitting, correlation and others.<sup>26</sup>

In the examples above the course of the boat was 0 deg or straight toward the sensor. The profile recognition capability was for our sensor parameters realistic up to incidence angles of about 60 deg relative to the boat length axis. For larger angles, a high range resolution is needed and the range features are also more limited as compared with smaller incidence angles.

The influence of beam jitter in the range waveforms was studied, and we conclude that a moderate beam jitter up to 0.25 mrad had a minor influence, while a large jitter 0.75 mrad (7.4% of the beam  $1/e^2$  divergence) decorrelated some pulses down to a value of 0.6 for the correlation coefficient. However, summing up several consecutive pulses will create a pulse which has a high correlation with the “library” waveform.

Waves corresponding to wind velocities up to 10 m/s and generated by a long fetch also led to moderate decorrelation. Higher sea states remain to be treated including adding the effect of foam and wet boats. The correlation matrix for consecutive range waveforms will reflect how the boat moves at the specific sea state at least for the tip-tilt behavior.

Atmospheric turbulence had a minor effect on the peak localizations in the range waveform as expected. However, the transverse resolution is reduced making the intensity image blurry.

The estimate of the width and height were quite sensitive to the range, which is probably connected to a higher SNR and larger number of pixels at the shorter ranges. The accuracy of the width and height were typically of the order of 1 to 2 m, which at least enables classification to different classes of boats.

For the 3-D matching,<sup>26</sup> we obtained good matching scores for the correct target-model match together with some false/confusing matches. The correct target-model match was within the top four for the three explored data sets. The confusing matches were made with models of similar dimensions and shape (w/o mast, high/low rail). For two targets data were only collected from the fore parts. For this type of matching, it is preferred to have target data that cover, although maybe sparsely, the complete target hull. When data is collected from only parts of the hull there is an increased risk for mismatches with models that contain similar parts although the overall shape of the model is

quite different. In spite of the poor data collection, for the two small targets we achieved correct target-model match that was within the top four.

Finally, from a system perspective all relevant information from the different sensors should be taken into account in the detection, classification and identification process. Radar and thermal IR may be natural for target detection due to their larger search capability. They can generate range and speed as well as courses for the vessels of interest. The radar and IR detections including their signatures are valuable data, which can support the laser system both in aiming and tracking as well as in the classification/ID process. The course for example will enable matching to the relevant range profile and width/height data. The speed is also of interest especially for the classification of small boats.

Analysis on laser data can incorporate 1-D, 2-D, and 3D data as discussed in Ref. 28. The combination of analysis of the 1-D, 2-D, and 3-D data need to be further studied in a data fusion context. For classification, there are a number of potential processing techniques which might be evaluated e.g., voting, multivariate statistics, principal component analysis, correlation analysis, and supervised/unsupervised learning.

#### Acknowledgments

This work was supported by the Swedish Armed Forces (FM). The authors thank Jimmy Berggren at FOI who helped characterizing the 3-D models used in the simulation.

#### References

1. F. Gini, A. Farina, and M. Greco, "Selected list of references on non-Gaussian radar detection," *IEEE T-AES* **37**(1), 329–359 (2001).
2. R. Ragnarsson et al., "Towards a combined sensor system for detection and classification of small surface vessels in the maritime domain," in *Radar 2012*, Glasgow (2012).
3. K. Krapels et al., "Midwave infrared and visible sensor performance modeling: small craft identification discrimination criteria for maritime security," *Appl. Opt.* **46**(30), 7345–7353 (2007).
4. A.N. de Jong et al., "Optical characteristics of small surface targets, measured in the False Bay, South Africa; June 2007," *Proc. SPIE* **7300**, 730003 (2009).
5. P. B. W. Schwing et al., "Optical characterisation of small surface targets," *Proc. SPIE* **6739**, 67390H (2007).
6. D. Bonnier, S. Lelievre, and L. Demers, "On the safe use of long-range laser active imager in the near-infrared for Homeland Security," *Proc. SPIE* **6206**, 62060A (2006).
7. O. David, R. Schneider, and R. Israeli, "Advance in active night vision for filling the gap in remote sensing," *Proc. SPIE* **7482**, 7482031 (2009).
8. O. Steinvall et al., "Laser imaging of small surface vessels and people at sea," *Proc. SPIE* **7684**, 768417 (2010).
9. P. Lutzmann, IOSB, private communication.
10. W. Armbruster and M. Hammer, "Maritime target identification in flash-ladar imagery," *Proc. SPIE* **8391**, 83910C (2012).
11. P. Lutzmann et al., "Laser vibration sensing: overview and applications," *Proc. SPIE* **8186**, 818602 (2011).
12. G. J. Kunz et al., "Detection of small targets in a marine environment using laser radar," *Proc. SPIE* **5885**, 5885F1 (2005).
13. J. C. van den Heuvel, R. M. Schoemaker, and H. M. A. Schleijsen, "Identification of air and sea-surface targets with a laser range profiler," *Proc. SPIE* **7323**, 73230Y1 (2009).
14. J. C. van den Heuvel, P. Pace, and O. Steinvall, "Laser opportunities in new naval missions," *Naval Forces* **29**(5), 46 (2008).
15. R. Schoemaker and K. Benoist, "Characterisation of small targets in a maritime environment by means of laser range profiling," *Proc. SPIE* **8037**, 803705 (2011).
16. O. Steinvall et al., "Measurement and modeling of laser range profiling of small maritime targets," *Proc. SPIE* **8542**, 85420I (2012).
17. T. Chevalier, "A ray tracing based model for 3D lidar systems," in *Proc. Int. Conf. on Comput. Graphics Theory Appl., GRAPP*, pp. 39–48, Vilamoura, Algarve, Portugal (2011).
18. T. R. Chevalier and O. K. Steinvall, "Laser radar modeling for simulation and performance evaluation," *Proc. SPIE* **7482**, 748206 (2009).
19. E. Jönsson et al., "Standoff lidar simulation for biological warfare agent detection, tracking and classification," *Proc. SPIE* **7665**, 766509 (2010).
20. <http://www.swan.tudelft.nl/>.
21. D. M. Tratt et al., "Airborne doppler Lidar investigation of the wind-modulated sea-surface angular retroreflectance signature," *Appl. Opt.* **41**(33), 6941–6949 (2002).
22. O. Steinvall, L. Sjöqvist, and M. Henriksson, "Photon counting lidar work at FOI," *Proc. SPIE* **8375**, 83750C (2012).
23. M. Henriksson et al., "Optical reflectance tomography using TCSPC laser radar," *Proc. SPIE* **8542**, 85420E (2012).
24. <http://www.3dcadbrowser.com/download.aspx?3dmodel=7024>.
25. C. Grönwall, F. Gustafsson, and M. Millnert, "Ground target recognition using rectangle estimation," *IEEE Trans. Image Process.* **15**, 3401–3409 (2006).
26. O. Steinvall and T. Chevalier, "Range accuracy and resolution for laser radars," *Proc. SPIE* **5988**, 598808 (2005).
27. O. Steinvall, L. Sjöqvist, and M. Henoiksson, "Photon counting lidar work at FOI, Sweden," *Proc. SPIE* **8375**, 83750C (2012).
28. O. Steinvall, T. Chevalier, and C. Grönwall, "Simulating the performance of laser imaging and range profiling of small surface vessels," *Proc. SPIE* **8731**, 87310U (2013).

**Ove Steinvall** received his MS degree in physics at the University of Uppsala in 1969 and a PhD in 1974 from Chalmers University. From 1977 to 2011 he led the Laser Group at FOI. Since 2011, he has been a senior laser expert at FOI. He is author of about 100 conference and journal articles and about 300 internal reports. He is a fellow of SPIE, and a member of OSA, the Swedish Optical Society and the Royal Academy of Military Sciences.

**Tomas Chevalier** received his MS in applied physics and electrical engineering in 2000. Since then, he has been working as a scientist at the Division of Information Systems, at the Swedish Defence Research Agency (FOI) in the field of laser-based sensing, where he performed his contributions to this paper. His main interest has covered 3-D signal processing for target recognition, data fusion, environment mapping, and sensor simulation. He is author or co-author of about 40 conference and journal articles. He is currently employed by SAAB Aeronautics.

**Christina Grönwall** received her MSc in computer science in 1992 and PhD in automatic control from Linköping University, Sweden, in 2006. She is currently working as a senior scientist at the Swedish Defence Research Agency (FOI), Sweden, and leading the sensor informatics group. Her research interests are in signal processing, geometric fitting, system modeling, and performance analysis of measurement systems, and particularly laser radar systems. She is currently a part-time guest researcher at the Automatic Control group, Linköping University, Sweden, and a member of SPIE.